Investigation of CO_2 reaction with copper oxide nanoparticles for room temperature gas sensing†

N. B. Tanvir,[ab] O. Yurchenko,*[a] Ch. Wilbertz[c] and G. Urban[ab]

The sensing of CO_2 at room temperature enables the prospects towards low power and low cost CO_2 gas sensors and has a high demand in both industrial and domestic applications. In this work we report a detailed work function read out (Kelvin probe) based analysis on copper oxide nanoparticles (CuO-NPs) as a new CO_2 gas sensitive material. The reversible interactions of CO_2 with the thick CuO-NPs layer result in a work function change of about 42 mV for dry air and approximately 97 mV for humid conditions (r.h. = 20%), at a CO_2 concentration step of 400 to 4000 ppm. The CO_2 gas sensing mechanism at room temperature is studied by Fourier transform infrared (FTIR) spectroscopy and explained by thermodynamical calculations. The correlation found between the FTIR spectrum and thermodynamical studies suggest the reversible formation of hydroxocarbonates (malachite, azurite) which is responsible for the gas sensing effect. Moreover, the results concerning long term signal stability over time present suitability towards indoor gas sensing applications. The results indicated in this paper give a new direction to metal oxide based nanoparticles as sufficiently fast and sensitive ambient CO_2 detecting materials.

Introduction

The sensing of CO_2 has attracted increasing attention for indoor applications in the past few decades. As the level of CO_2 is one of the dominant factors for comfortable indoor climate, the sensing of CO_2 plays an important role for controlled heating, ventilation and air conditioning (HVAC) systems. The maintenance of high indoor air quality (iAQ) also requires huge amount of energy consumption, thus the optimization of energy consumption is also an important factor to be considered. The HVAC systems of vehicles, operated in the recirculation mode can result in high accumulation of CO_2 within the vehicle cabin. The exposure to high CO_2 concentrations for a long period of time can cause problems such as dizziness or headache and it can go up to severe health problems such as breathing difficulties and unconsciousness.[1,2]

Metal oxide based high temperature CO_2 gas sensors have been intensively studied in the past due to their relatively straightforward working principle and easy implementation towards micro-electronic devices.[2–4] The concept of sensing for various gases is typically based on the detection of conductivity changes within the gas sensitive material.[5–9] However, apart from the conductivity change, measurements based on the change in capacitance, mass, work function and also optical properties can be utilized effectively to detect the reversible interaction of the gas with the sensing materials.[10]

Considering the high demand to move towards the low cost-performance ratio, gas sensing field effect transistors (gas FETs) operating at low temperature may play a significant role.[11] The working principle of gas FETs is based on the work function (WF) change of a gas sensitive material deposited on a transistor gate, upon the change in ambient atmosphere.[12] The simple investigation of WF-changes can be performed using Kelvin probe (KP) measurements which give the "contact potential difference" (CPD) between the electrically connected reference electrode and the material to be investigated.[13,14] One of the advantages of WF based gas sensing devices is the possibility to use a large variety of gas sensitive materials such as metallic conductors, semiconductors, and even insulators.[15,16]

Since CO_2 is a thermodynamically very stable gas and the chemical reaction of the gas sensitive layer with the gas analyte is not favorable, there exist only few materials showing a reaction to CO_2 that could result in gas detecting signals.[17] For example, Ostrick *et al.* investigated different carbonates and showed the highest sensitivity for $BaCO_3$ as the CO_2 sensing material.[18] Similarly Stegmeier *et al.* indicated hetero-polysiloxanes as the CO_2 sensing layer.[19] The sensors based on these materials usually suffer from limited accuracy in the desired CO_2 concentration range and lack of long term signal

[a]*Freiburg Materials Research Center, University of Freiburg, Stefan Meier Straße 21, 79104 Freiburg, Germany. E-mail: olena.yurchenko@fmf.uni-freiburg.de; Tel: +49 7612034781*

[b]*Laboratory for Sensors, Department of Microsystems Engineering, University of Freiburg, Georges Köhler Allee 103, 79110 Freiburg, Germany*

[c]*Micronas GmbH, Wafer Process Integration, Hans Bunte Strasse 19, 79108 Freiburg, Germany*

† Electronic supplementary information (ESI) available: Instrumentation, XRD, SEM, thermodynamical investigations. See DOI: 10.1039/c5ta09089j

5294 | *J. Mater. Chem. A*, 2016, 4, 5294–5302

This journal is © The Royal Society of Chemistry 2016

stability mainly due to an incomplete reversible interaction of the gas with the surface of the sensing material.[4] Thus it can be stated that the reversibility of gas interaction with the metal oxide surface is the main hurdle to achieve and has a lot of potential for research. The more stable metal oxides or related materials, such as LaOCl, and SnO_2 modified with LaOCl, $Nd_2O_2CO_3$, $La_{1-x}Sr_xFeO_3$, Ba_xWO_y, and $BaCeO_3$, that have so far been investigated for resistive or capacitive type of sensors operated at higher temperatures, exhibit comparably low sensitivity towards CO_2.[6–9,20,21] Thus as a consequence, expensive and bulky non-dispersive infrared (NDIR) sensors are considered to be the state of the art for CO_2 sensing.[22]

The utilization of pure metal oxide nanoparticles is a relatively new approach towards gas sensing. We found on the basis of Kelvin probe investigations that CuO-NPs based layers feature high work function response towards CO_2 at low temperatures.[23,24] The focus of this study is set on the investigation of possible sensing mechanism and the understanding of the reactions on the basis of thermodynamic considerations taking place at the CuO-NPs surface by CO_2 exposure at room temperature. Moreover a detailed examination of the humidity and layer thickness influence on the WF-response along with WF signal stability over time is also presented which is typically important considering the applications towards the sensor industry.

Experimental

Work function measurements were performed on a locally developed Kelvin probe setup. The lock-in Kelvin probe with a reference electrode made up of a gold grid and having a diameter of 3 mm along with the Kelvin control unit were procured from Besocke Delta Phi. The Kelvin control unit was used to adjust the vacuum level of the CuO-NPs layer by applying an additional backing potential V_B, when brought into electrical contact with the reference electrode and exposed to CO_2. The applied V_B is exactly the negative of CPD and was used to calculate the work function change of CuO-NPs after calibration with respect to the Au reference electrode. Both the sample and the reference electrode were mounted at a distance of 2 mm in a grounded steel chamber. The gas concentrations were controlled with the help of precise mass flow controllers (MFCs) procured from Bronkhorst. All the measurements were carried out with a constant overall gas flow of 1000 ml min^{-1} and in synthetic air having an oxygen to nitrogen ratio of 20 : 80%.

For the Kelvin probe measurements silicon substrates having a size of 4 × 4 mm were used. The substrates were initially sputtered with 200 nm thick titanium nitride (TiN). The conductive and inert nature of TiN makes it suitable to act as a backing electrode in the case of work function type CO_2 gas sensors. The CuO-NPs, having a particle size of around 50 nm, were dispersed in an aqueous solution and drop-coated on the TiN substrate and the sample was dried for 15 minutes at 100 °C after deposition.

The microstructure of CuO-NPs was investigated by X-ray diffraction (XRD) spectroscopy and the morphology of CuO-NPs

films along with porosity was analyzed by scanning electron microscopy (SEM). XRD measurements were carried out using a Siemens D-5000 diffractometer with Cu-Kα radiation and SEM images were taken using a Quanta FEG 250. Fourier transform infrared (FTIR) spectra were recorded using a Nicolet Magna-IR 760 spectrometer with the software OMNIC.

Results and discussion

Material characterization

The investigated CuO-NPs are nanocrystalline with a tenorite structure which was confirmed by XRD spectra (ESI, Fig. S1†). The SEM image (Fig. S2†) indicates an aggregation, which is typically observed with nanoparticles having a spherical-type morphology.[25] A highly porous layer is generated by the aggregation of CuO-NPs. The CuO-NPs film includes macropores (size > 50 nm) which should enable fast gas diffusion inside the films and fast response as well as mesopores (2–50 nm), which provide high surface area and high number of reaction sites for gas interaction. Micrometer-sized CuO usually exhibits low porosity and surface area.

The layer composition and the present surface species were investigated by FTIR spectroscopy. The FTIR technique has been commonly used in catalysis research,[26] CO_2 capture[27] and gas sensing,[21,28,29] in order to investigate the gas interactions with the catalyst, adsorbent or for studying the gas sensing mechanism and thermodynamics of weak solid–gas interactions.[30] The main advantage of FTIR is the possibility to perform measurements under ambient or gas sensing conditions; no vacuum is needed. Moreover, in contrast to XRD, FTIR can also identify amorphous components, which are preferably formed at low temperatures. Since it is known that metal oxide layers absorb and accumulate water,[31] as well as humidity has an effect on work function based CO_2 response of CuO,[24] the FTIR spectrum of CuO-NPs was taken in ambient air after layer preparation without further treatment and after drying at 100 °C for 24 h (Fig. 1).
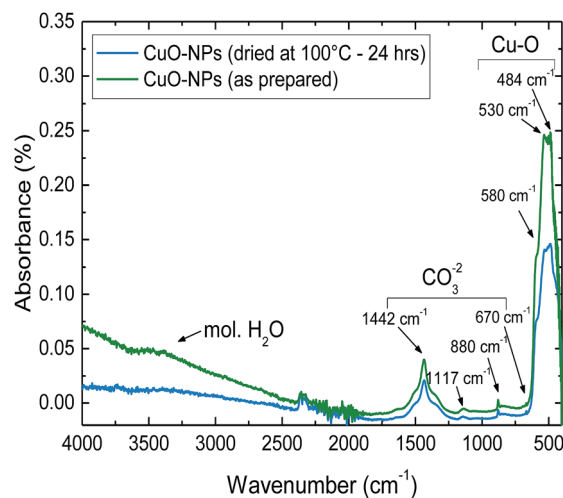

Fig. 1 FTIR spectrum of the as-deposited CuO-NPs layer in comparison to CuO-NPs dried at 100 °C for 24 h.

The FTIR spectrum of the as-prepared CuO-NPs sample shows vibrations of CuO characteristic absorption peaks at the vibration average wave numbers of 480, 530 and 580 cm^{-1}.[32] Moreover, the fundamental modes of the carbonate ion group arising from the in-plane bending, out-of-plane bending, symmetric stretching and asymmetric stretching at the average wave numbers of 685, 880, 1117 and 1442 cm^{-1} are also detected.[33] The broad band belonging to hydroxyl-stretching and adsorbed water is observed in the region between 3000 and 4000 cm^{-1}.[34]

The comparison of the FTIR spectrum for the dried and non-dried CuO-NPs layer reveals that in dried samples only the broad band representing molecular adsorbed water is absent. However, chemisorbed hydroxyl groups should be present after treatment at this temperature. Usually, surface OH$^-$ groups start to desorb at temperatures higher than 400 °C.[31,35] Moreover, the existence of carbonate groups lead to an assumption that in ambient air with the background CO$_2$ concentration of 400 ppm a thin carbonate layer is formed on the surface of CuO-NPs.

Gas sensing characterization

The gas sensitivity of CuO-NPs layers was investigated with the help of the Kelvin probe method. The KP method enables the detection of the surface charge alteration due to interactions with a gas through the measurement of the change in contact potential difference (CPD) between the gas sensitive material and the reference electrode. The CPD value, in turn, can be used to evaluate the WF-change of the sensitive layer under consideration. Thus in order to investigate the changes in WF for different gas exposures, the reference electrode needs to be gas inert.[13,36]

CO$_2$ exposure was varied in the range of 400 to 4000 ppm, considering 400 ppm as the CO$_2$ background in atmosphere. In order to investigate the effect of humidity, the relative humidity levels were varied in the range of 0 to 60%.

Initially the detailed investigation of humidity and layer thickness effect on CO$_2$ sensing behavior of CuO-NPs was conducted. The WF-change of CuO-NPs when exposed to CO$_2$ along with varying CuO-NPs layer thickness and changing relative humidity (r.h.) is depicted in Fig. 2.

The KP measurements indicate the reversible change in WF-response for CuO-NPs to CO$_2$ exposure of 400 to 4000 ppm at room temperature. The signal height of WF-response to CO$_2$ exposure is found to be sensitive to both humidity and layer thickness. In the case of the thick CuO-NPs layer (h_{CuO} = 100 μm), CO$_2$ exposure under dry conditions lead to smaller WF-change ($\Delta\Phi_{p_{CO_2}=4000}$ = 42 mV). But the inclusion of humidity (r.h. = 20%) results in the enhancement of the WF-response ($\Delta\Phi_{p_{CO_2}=4000}$ = 97 mV). The thin CuO-NPs layer (h_{CuO} = 3 μm) reveals significantly lower WF-response under both dry ($\Delta\Phi_{p_{CO_2}=4000}$ = 15 mV) and humid ($\Delta\Phi_{p_{CO_2}=4000}$ = 41 mV at 20% r.h.) conditions. The increment of CO$_2$ response with increasing water concentration is the first indication for the involvement of water in the CO$_2$ sensing process. Thus assuming that the CuO-NPs layer can accumulate water, the
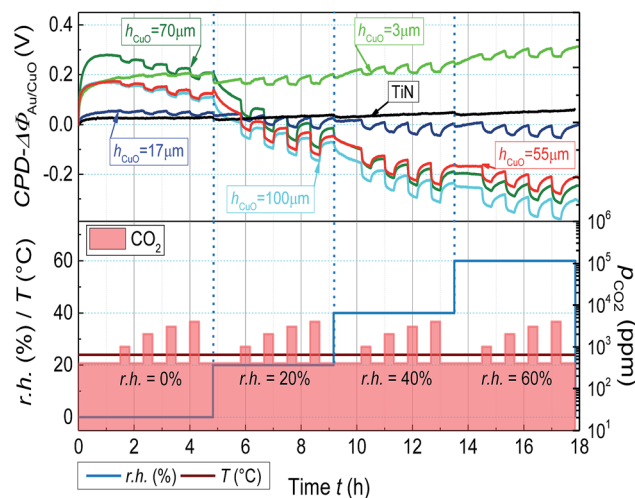

Fig. 2 Change in WF of CuO-NPs layer due to CO$_2$ exposure in the range of 400 to 4000 ppm with varying r.h. CO$_2$ is introduced into the chamber for 20 min with the relaxation time of 30 min.

experiment was repeated after the drying of the sample at 100 °C for 24 h.

As expected, the dried layer showed nearly no reaction to CO$_2$ under dry conditions (Fig. 3). Since according to the FTIR results (Fig. 1), the dried film contains nearly no adsorbed molecular water, the smaller signal further endorses the importance of humidity for the layer interaction with CO$_2$. Another interesting result is the detection of decrease in WF-response with the increase in humidity from a certain level (r.h. ≥ 40%, Fig. 2). One conceivable reason for the decrease in WF-response can be the formation of the water film which decelerates the diffusion of CO$_2$ towards the gas active centers.

The response (t_{90}) and the recovery (t_{10}) times of the thick CuO-NPs layer have been found out to be higher when exposed
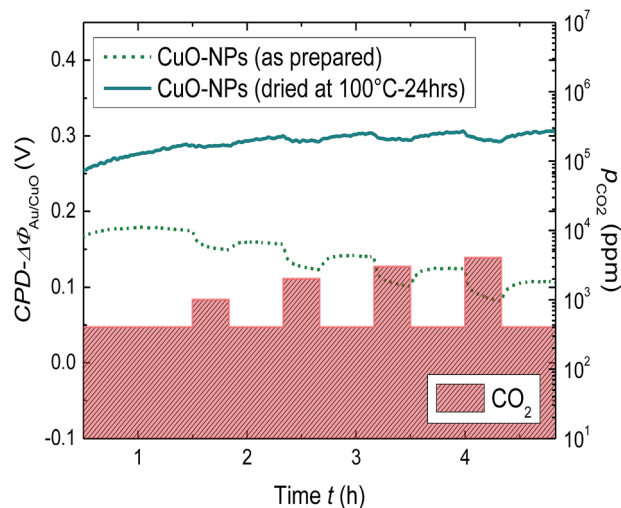

Fig. 3 Comparison of the change in WF for the thick CuO-NPs layer dried at 100 °C for 24 h and not dried, due to stepwise CO$_2$ exposure from 400 to 4000 ppm.

to CO_2 under dry conditions ($t_{90} \approx 720$ s, r.h. = 0%) as compared to humid conditions ($t_{90} \approx 500$ s, r.h. = 20%) (ESI, Fig. S4†). The decrease in work function response time under humid conditions further emphasizes the importance of humidity for work function based CO_2 sensing using CuO-NPs. Moreover, since the CuO-NPs layers are highly porous, it can be assumed that the high response times are provoked by the slow reaction kinetics. However, we realize the importance of response and recovery times from the sensor application point of view and intend to perform detailed investigations for the optimization of work function signal response by using a combined effect of humidity, thickness and low temperatures (till 100 °C).

The WF-response comparison of CuO-NPs with the layer thickness (3 μm ≤ h_{CuO} ≤ 100 μm) under dry and humid (r.h. = 20%) conditions is shown in Fig. 4. A clear decrease in WF-response is detected for decreasing layer thickness. The dependence of WF-change on the layer thickness confirms that the gas interactions take place essentially on the sensitive layer's surface as the surface of the thicker porous films is larger. However for the layers thicker than 60 μm, the gas accessible surface reaches its maximum limit and thus no further increase in signal height can be achieved.

Thermodynamical investigations of the gas sensing reaction

In the surface reactions of metal oxides with gases, the adsorbed water plays an important role.[4,31,35] Also in the case of CO_2, a strong effect of humidity on CO_2 sensing has been found for all investigated materials, $BaCO_3$, $LaOCl$, $SnO_2/LaOCl$, $Nd_2O_2CO_3$, Ba_xWO_y, $BaCeO_3$, and explained by the formation of different carbonate related species on the surface.[6–8,18,20,21,37] In the case of $BaCO_3$, the dependency of CO_2 sensing on relative humidity in the environment and the change in WF for CO_2 exposure was attributed by Ostrick et al. to a reaction which resulted in the formation of dimeric HCO_3^- which requires the presence of water.[18,37] Based on the investigations by Ostrick

et al., the same reaction was also assumed by Cavanagh et al. for the Ba_xWO_y sensing layer.[20] In the case of $LaOCl$, $BaCeO_3$, and $Nd_2O_2CO_3$, the detection of CO_2 is described by the interaction of CO_2 with OH^-/O^{2-} groups present at the surface of these materials. It has been discussed and partially confirmed that the concentration of OH^- groups on the surface is correlated with the humidity level in the environment.[6–8,21] These types of interactions lead to the formation of carbonate and hydroxocarbonate species on the surface with the general formula $M_x(OH)_y(CO_3)_z$ with M for the metal. However, the optimal conditions for CO_2 sensing are reported to be only higher temperatures (T > 250 °C).

According to FTIR results, it may be assumed that a similar kind of reaction as in the case of $BaCO_3$ takes place on the surface of CuO-NPs. Thus, the change in WF for CuO-NPs in the presence of humidity and CO_2 can be explained with the help of the following reaction path (Scheme 1):

$$CuO_{(s)} + CO_{2 (g)} \rightleftharpoons CuCO_{3 (s)}$$

$$CuCO_{3(s)} + CO_{2(g)} + H_2O \rightleftharpoons Cu(HCO_3)_{2(s)}$$
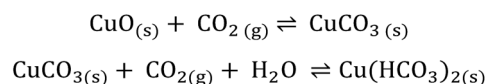
Scheme 1 Mechanism explanation through the formation of hydroxycarbonate.

With the help of Scheme 1, it can be predicted that the initially formed thin layer of copper carbonate $CuCO_3$ on the surface reacts to produce copper hydrogen carbonate $Cu(HCO_3)_2$ in the presence of CO_2 and H_2O. The carbonate species on the CuO-NPs surface refer indirectly to this reaction path. However to assess the possibility of this reaction path, we found in the literature and also calculated the standard Gibbs free energy change ($\Delta_R G°$) for the formation of $CuCO_3$, which suggests if the reaction is possible under standard conditions (298.15 K, 1 bar) or not. The standard Gibbs free energy change for the reactions is given by:

$$\Delta_R G° = \sum \Delta_f G°_{prod} - \sum \Delta_f G°_{educt} \qquad (1)$$

where $\Delta_f G°_{prod}$ is the standard Gibbs free energy of formation of all products and $\Delta_f G°_{educt}$ is the standard Gibbs free energy of formation of all educts.

For the calculations of $\Delta_R G°$, the values of standard Gibbs free energy of formation from Table 1 were used and the calculation results are summarized in Table 2.
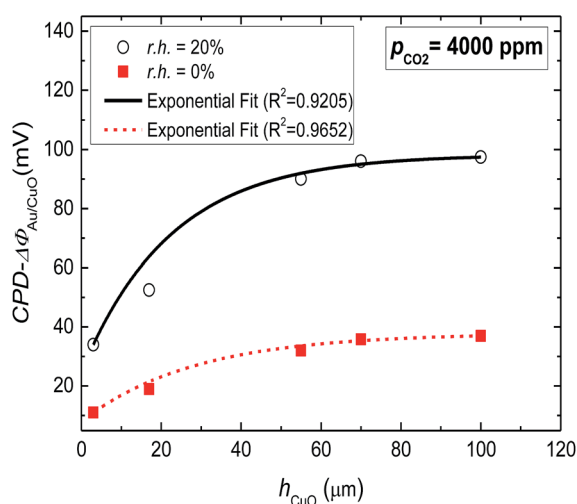

Fig. 4 The dependence of WF-response ($\Delta\Phi$) on CuO-NPs layer thickness under dry and humid conditions.

Table 1 Gibbs free energy of formation of chemical compounds under standard conditions, T = 298.15 K, p_{CO_2} = 1 bar

Species	Formula	$\Delta_f G°$ (kJ mol^{-1})
Tenorite (s)[38]	CuO	−129.7 ± 2.1
Copper carbonate (aq)[38]	CuCO$_3$(aq)	−501.3 ± 0.6
Malachite (s)[38]	Cu$_2$(OH)$_2$CO$_3$	−903.3 ± 1.2
Azurite (s)[38]	Cu$_3$(OH)$_2$(CO$_3$)$_2$	−1434.2 ± 1.8
Carbon dioxide (g)[39,40]	CO$_2$	−394.37
Carbon dioxide (aq)[40]	CO$_2$	−385.99
Water (l)[39]	H$_2$O	−237.1

This journal is © The Royal Society of Chemistry 2016
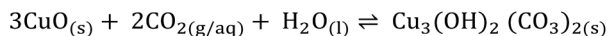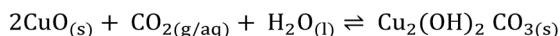
J. Mater. Chem. A, 2016, 4, 5294–5302 | 5297

Table 2 Gibbs free energy of the reaction under standard conditions, $T = 298.15$ K, $p_{CO_2} = 1$ bar

Reaction	$\Delta_R G^\circ$ (kJ mol^{-1})
$CuO(s) + CO_2(g) \rightarrow CuCO_3(s)$	+4.9 (ref. 41) or +4.2 (ref. 42)
$2CuO(s) + CO_2(g) + H_2O(l) \rightarrow Cu_2(OH)_2CO_3(s)^a$	−12.4
$2CuO(s) + CO_2(aq) + H_2O(l) \rightarrow Cu_2(OH)_2CO_3(s)^a$	−20.7
$3CuO(s) + 2CO_2(g) + H_2O(l) \rightarrow Cu_3(OH)_2(CO_3)_2(s)^a$	−19.2
$3CuO(s) + 2CO_2(aq) + H_2O(l) \rightarrow Cu_3(OH)_2(CO_3)_2(s)^a$	−35.9

[a] The calculations are carried out according to eqn (1) using the data from Table 1.

According to Isahak *et al.* and Seidel *et al.*, the value of Gibbs free energy for the reaction resulting in the formation of CuCO$_3$ is given by +4.9 kJ mol^{-1} and +4.2 kJ mol^{-1}, respectively, at 298 K and $p_{CO_2} = 1$ bar (Table 2).[41,42] Consequently, the reaction of carbonate formation is thermodynamically unfavorable under the standard conditions.

The second possible reaction scheme involves the formation and decomposition of basic copper carbonate or hydroxocarbonate structures. Due to its instability, CuCO$_3$ takes a special position within the group of simple carbonates M$_{II}$CO$_3$ (M from Mg till Zn).[42] However, the presence of humidity can cause the formation of different kinds of carbonates. The existence of Cu(II) in nature is normally in the form of basic carbonates malachite or azurite.[42,43] Thus one can predict the formation of malachite or azurite related structures (Scheme 2) by CO$_2$ adsorption on the CuO surface in the presence of humidity:

$$2CuO_{(s)} + CO_{2(g/aq)} + H_2O_{(l)} \rightleftharpoons Cu_2(OH)_2\,CO_{3(s)}$$

$$3CuO_{(s)} + 2CO_{2(g/aq)} + H_2O_{(l)} \rightleftharpoons Cu_3(OH)_2\,(CO_3)_{2(s)}$$

Scheme 2 Mechanism explanation through the formation of hydroxocarbonate.

It has to be taken into account that Scheme 2 expresses the overall process; the elementary reaction steps are not described here. However for the thermodynamical considerations, the reactions with defined reactants and educts are required.

According to Fig. 1, the adsorbed molecular water or water in the form of the water film can be identified on top of the CuO-NPs surface. Due to the existence of the water film, it is reasonable to assume that CO$_2$ molecules can be solvated by water molecules. For the sake of comparison, two cases, one with CO$_2$ as gas (g) and another with solvated CO$_2$(aq) (Table 1) are considered in calculations of standard Gibbs free energy of reactions $\Delta_R G^\circ$ (Table 2). It is shown in Table 2 that $\Delta_R G^\circ$ for the formation of malachite or azurite-like structures, even at CO$_2$ partial pressure (p_{CO_2}) of 1 bar is relatively small for both cases (−12.4 or −20.7 9 kJ mol^{-1} and −19.2 or −35.9 kJ mol^{-1}, respectively). The CO$_2$ molecules in gaseous as well as in solvated state are able to react with the CuO-NPs surface under the formation of hydroxocarbonates. The small $\Delta_R G^\circ$ values

mean that both reactions regardless of the CO$_2$ state are very sensitive to p_{CO_2}. In accordance with Vink *et al.*, the equilibrium p_{CO_2} for the transition of CuO to malachite is about 360 ppm (CO$_2$(g)), which is close to the atmospheric conditions.[43] Beyond this value, the malachite structures are present on the CuO surface and their extent is defined by p_{CO_2}. For CO$_2$ gas sensing measurements, relevant p_{CO_2} values start from 400 ppm (background CO$_2$ concentration in air) and reach 4000 ppm. In order to assess the driving force behind these reactions we calculated $\Delta_R G$ values for the formation of hydroxocarbonates species at three p_{CO_2}, 400, 1000 and 4000 ppm.

The Gibbs free energies $\Delta_R G$ for the reaction of the formation of malachite (eqn (2)) and azurite (eqn (3)) taking place at 298.15 K and partial pressures of CO$_2$ differing from 1 bar were calculated by the following equations:

$$\Delta_R G = \Delta_R G^\circ + RT \ln(p_{CO_2})^{-1} \quad (2)$$

$$\Delta_R G = \Delta_R G^\circ + RT \ln(p_{CO_2})^{-2} \quad (3)$$

where $R = 8.314$ J mol^{-1} K^{-1} is the ideal gas constant, T is the temperature in kelvin, p_{CO_2} is the partial pressure of CO$_2$. For more information concerning the derivation of these equations, see ESI, eqn (S1)–(S4).†

The partial pressure of water is not considered in calculations since according to FTIR results, water molecules exist as a water film on the CuO surface ($p_{H_2O} = 1$). Additionally, both possible conditions for CO$_2$ were examined, CO$_2$ in gaseous state CO$_2$(g) and in solvated state CO$_2$(aq). The calculation results are listed in Table 3.

With the help of these calculations it can be concluded that the reactions with gaseous CO$_2$ are not favorable at low CO$_2$ partial pressures, which are valid for sensor operating conditions ($\Delta_R G > 0$ for p_{CO_2} between 400 and 4000 ppm, Table 3). However when we consider that CO$_2$ exists on the CuO surface in the solvated state (aq), a thermodynamically favorable reaction is expected. CO$_2$ can also exist on the CuO-NPs surface in the adsorbed state; but the thermodynamical data for adsorbed

Table 3 Gibbs free energy of reactions at $T = 298.15$ and different CO$_2$ partial pressures

Reaction	p_{CO_2} (ppm)	$\Delta_R G$ (kJ mol^{-1})
$2CuO(s) + CO_2(g) + H_2O(l) \rightleftharpoons$ $Cu_2(OH)_2CO_3(s)^a$	400	+7.0
	1000	+4.8
	4000	+1.4
$2CuO(s) + CO_2(aq) + H_2O(l) \rightleftharpoons$ $Cu_2(OH)_2CO_3(s)^a$	400	−1.4
	1000	**−3.6**
	4000	**−7.0**
$3CuO(s) + 2CO_2(g) + H_2O(l) \rightleftharpoons$ $Cu_3(OH)_2(CO_3)_2(s)^a$	400	+19.7
	1000	+15.2
	4000	+8.2
$3CuO(s) + 2CO_2(aq) + H_2O(l) \rightleftharpoons$ $Cu_3(OH)_2(CO_3)_2(s)^a$	400	+2.9
	1000	−1.6
	4000	**−8.6**

[a] The data shown in this table are calculated according to eqn (2) and (3) along with $\Delta_R G^\circ$ listed in Table 1. $\Delta_R G$ given in bold represents the favorable reaction process under the given conditions.

5298 | *J. Mater. Chem. A*, 2016, **4**, 5294–5302

This journal is © The Royal Society of Chemistry 2016

CO_2 is not available. Moreover we assume that in both cases, Gibbs energy of formation $\Delta_f G°$ is reduced in comparison to $\Delta_f G°$ for free CO_2, due to weakening of binding in the molecule as a result of interactions (compare $\Delta_f G°$ for $CO_2(aq)$ with $CO_2(g)$, Table 1). This reduction in $\Delta_f G°$ enables the reaction with CO_2 already at low partial pressures. According to our calculations, $\Delta_R G$ values for the reaction of malachite formation at 400, 1000 and 4000 ppm CO_2 partial pressures are −1.4, −3.6 and −7.0 kJ mol^{-1} and for azurite formation +2.9, −1.6 and −8.6 kJ mol^{-1}, respectively. The increase in reaction energy $\Delta_R G$ for the formation of malachite-like structures on the CuO-NPs surface with the increasing p_{CO_2} (from −1.4 to −3.6 kJ mol^{-1}) indicates the rise in driving force towards malachite formation. In contrast, the formation of azurite-like structures is only possible at higher p_{CO_2}. As shown in Table 3, only at 4000 ppm, $\Delta_R G$ for the reaction of azurite formation (−8.6 kJ mol^{-1}) is larger than $\Delta_R G$ of malachite formation (−7.0 kJ mol^{-1}) and thus the probability of azurite formation at this particular p_{CO_2} is higher. To conclude it can be stated that the increase in $\Delta_R G$ at higher p_{CO_2} indicates the formation of more carbonate species on the CuO-NPs surface and results in the altering of work function. The comparison of the FTIR spectrum for the CuO-NPs layer (Fig. 1) with the spectrum of thermally treated azurite from the literature reveals substantial similarities between both the spectra.[34] This comparison underlines the statement that the formations of basic carbonates on the CuO surface are the key reactions happening in this case. The small values of $\Delta_R G$ for these reactions at the CO_2 background concentration ensure the reversible process which is necessary for the equilibrium type gas sensors. In this case, the stability of products is not high and equilibrium is influenced by p_{CO_2}.

We are aware that $\Delta_R G°$ values for bulk materials are not identical with energies for the formation of surface layers and partially considered this by the introduction of solvated $CO_2(aq)$. Additionally, the surface energies on the nanoparticle surface can differ significantly from those on the flat surface. Furthermore, we considered in our calculations water only as the molecular water film. Separately adsorbed single H_2O molecules or OH^- groups (which is expected for the measurements at higher temperature), will provide other values for $\Delta_R G°$. A small $\Delta\Phi$-response value detected in dry air for the dried sample (Fig. 3) indicates that the reaction with participation of exclusively hydroxyl groups on the surfaces takes place to a lesser extent than in the presence of molecular water. The presented reactions describe well the CO_2 interactions with the CuO-NPs surface at room temperature and the reaction is found out to be reversible.

In summary, it can be pointed out that CuO reacts with CO_2 and H_2O in a similar manner as La_2O_3, $LaOCl$, $BaCeO_3$ or $Nd_2O_2CO_3$, which were investigated for resistivity based gas sensing. However, in the case of CuO due to the differences in thermodynamics, the optimal conditions for the reaction and thus the operation conditions as well as the process reversibility are found to be different that can open up new prospects for CO_2 gas sensing at low temperature range. A short comparison of the $\Delta\Phi$-response of CuO-NPs to the other published materials for CO_2 gas sensing is depicted in Table 4.

Table 4 Comparison of different materials investigated for work function readout based CO_2 gas sensing using the Kelvin probe

Material	$\Delta_{p CO_2}$ (ppm)	r.h. (%)	$\Delta\Phi$ (mV)
$BaCO_3$ (ref. 18 and 37)[a]	400 → 5000	40	55
Mg-MOF-74 (ref. 44 and 45)[a]	400 → 4000	50	5–8
Co-MOF-74 (ref. 44 and 45)[a]	400 → 4000	50	5–8
(Hetero-)polysiloxanes[19a]	400 → 4000	40	15–20
Nanocrystalline CeO_2 (ref. 46)[a]	400 → 4000	30	80
CuO-NPs (this study)[a]	400 → 4000	20	97

[a] The work function values mentioned here are the maximum measured values for the respective material under optimized conditions ($\Delta_{p CO_2}$, r.h.) at room temperature.

Stability of gas sensitive CuO-NPs layers

So far we have demonstrated that CuO-NPs reveal sensitivity towards CO_2. However the implementation towards sensor applications requires short and long-term stability in gas sensing properties of the layer.

In order to investigate the short term stability, the CuO-NPs layer was treated with a serial CO_2 gas cycles of 4000 ppm for a short period of time along with the constant humidity level of 30% and the Kelvin probe measurements are shown in Fig. 5. After the first cycle of CO_2 exposure, the drift in the signal appears to have settled down (returning of the signal back to the base line) and showed the WF-response of approximately 80 mV. The change in WF-response for the rest of the cycles appeared at the same level, thus indicating the stability and reproducibility of the gas sensing process for the short term measurements.

For long term gas sensing stability investigations, the Kelvin probe samples containing the CuO-NPs layer was stored under normal laboratory conditions after the first CO_2 sensing measurement and was measured again three times with an interval of 1 month.
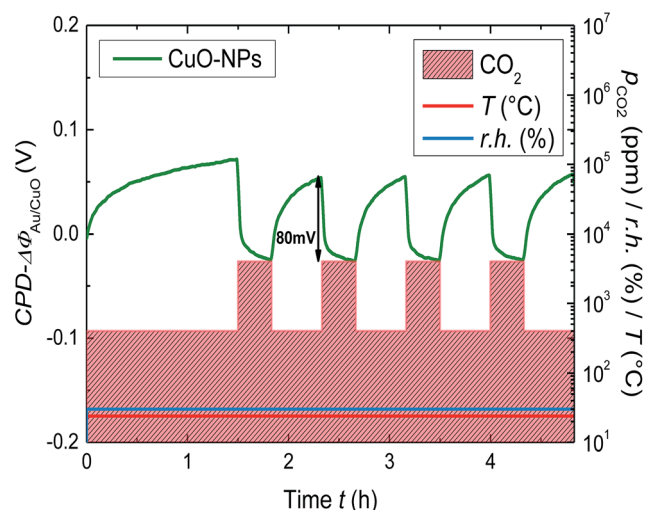

Fig. 5 Change of the WF for the CuO-NPs layer due to the serial CO_2 exposure of 400 to 4000 ppm at r.h. = 30% and room temperature.

In Fig. 6, the Kelvin probe measurement showing the long term work function signal stability is depicted. The CuO-NPs were exposed to CO_2 in a step kind of profile, with CO_2 concentration incrementing at 1000 ppm till 5000 ppm, after starting at the base concentration of 400 ppm. The effect of humidity on the long term CO_2 sensing has been investigated by humidity variation in the range of 30% to 80%. CuO-NPs showed the biggest change in WF-response for the fresh sample (1st part). After one month a slight reduction in the signal height (2nd part) and after the 2nd month (3rd and 4th part) no reduction in signal height have been detected. It can be concluded that CuO-NPs when exposed to CO_2 need some time to settle at the beginning. However, over time the gas sensing process stabilizes and results in the reversible reaction at the surface.

A comparison of the time dependent WF-response with respect to humidity is depicted in Fig. 7. All the measurements are base line corrected in order to obtain an easy comparison. The first measurements performed after deposition at the r.h. of 30, 60 and 80% showed the change in WF-response of about 53, 58 and 48 mV, respectively. However the recovery of the signal back to the baseline is not detected for all the cases, indicating the slow desorption of CO_2 as compared to the adsorption. It is interesting to notice that after attaining the constant level the change in WF-response is no more dependent on r.h. during CO_2 exposure. One possible reason for this phenomenon could be related to the humidity capturing capability of the CuO-NPs layer. The CuO-NPs layers have a saturation limit to capture humidity and once this level has been reached, the dependence of CO_2 sensing on r.h. is no more visible. The absolute value of the measurements as depicted in Fig. 2, 4 and 5 compared to Fig. 6 and 7 differ significantly. That might be due to the waiting time between the layer deposition and the first measurement; however this phenomenon has to be clarified in future.
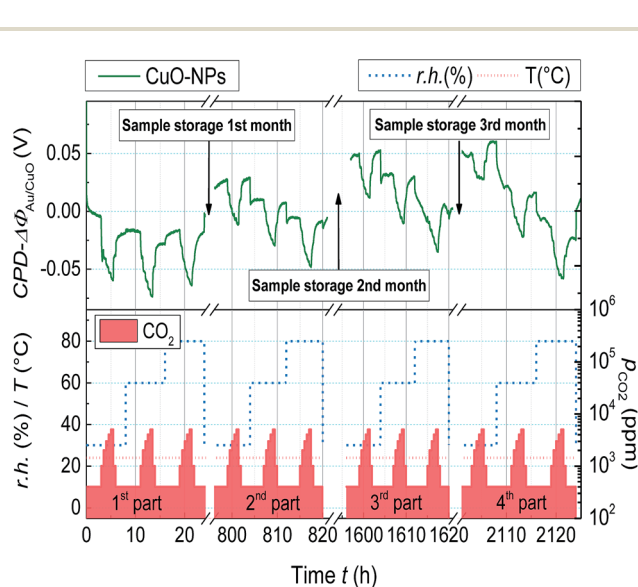

Fig. 6 Change of the WF for the CuO–NPs layer due to CO_2 exposure (400 ppm $\leq p_{CO_2} \leq$ 5000 ppm) with varying r.h. (30% $\leq$ r.h. $\leq$80%) and measured with an interval of one month.
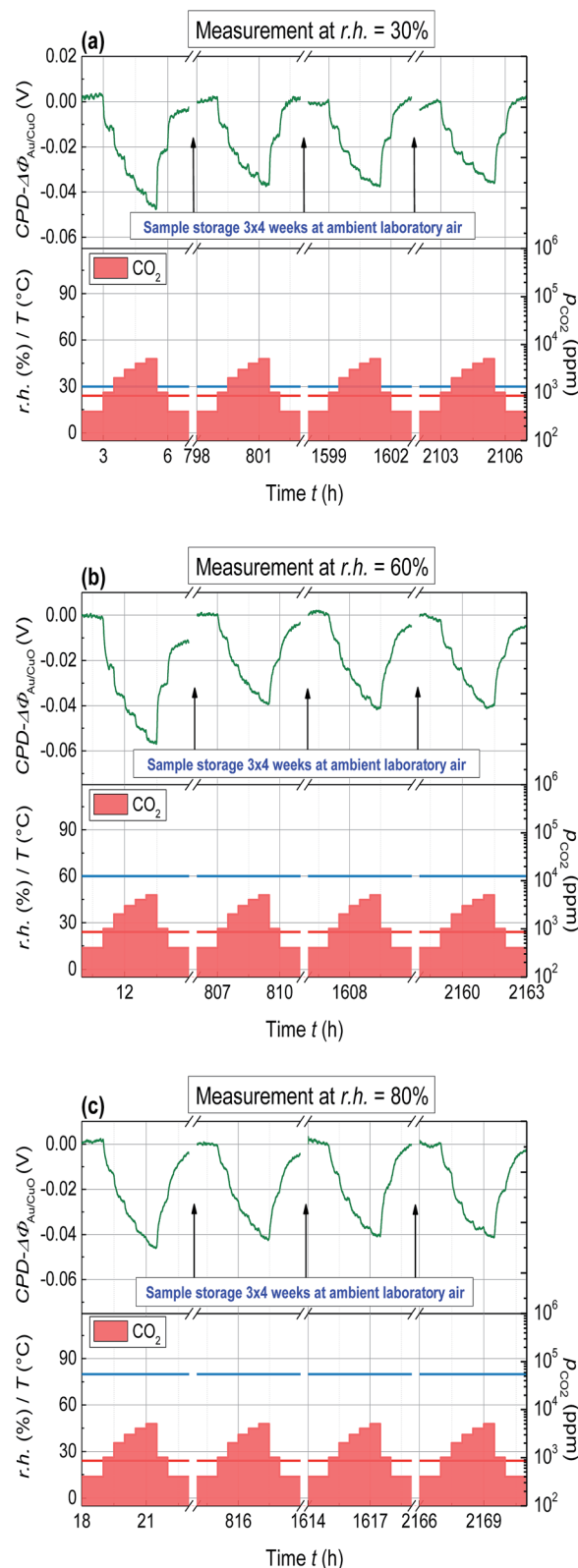

Fig. 7 (a) The time dependent response of WF measured at a constant r.h. level of 30%; (b) 60%; (c) 80%. The sample is exposed to CO_2 in the range of 400 to 5000 ppm for the duration of 3 months having an interval of 1 month between each measurement.

Conclusions

The special properties of CuO-NPs with respect to CO_2 gas sensing at room temperature were investigated with the help of work function (Kelvin probe) based readout. The formation of hydroxocarbonate species (malachite and azurite) as a main reaction leading to the change in work function was proved with the help of FTIR measurements and thermodynamical considerations. Our Kelvin probe results and thermodynamical studies indicate that the presence of humidity plays a significant role in the interaction of CO_2 with CuO-NPs. Although the presence of humidity is necessary for the reaction of CO_2 with CuO, this presence when increased from a certain level (r.h. $\geq$ 40%) has a negative impact on the work function change. The smaller work function change might be associated with the formation of the water film on the nanoparticle surface which decelerates the diffusion of CO_2 towards gas-active centres. Moreover, the investigations concerning the layer thickness dependency on CO_2 sensing indicated enhancement in the signal with increasing layer thickness. However, the signal saturated at about 60 μm, and no further layer thickness dependency on work function response was detected beyond 60 μm. Finally the investigated layers presented impressive long term signal stability over a measurement period of 3 months which is a necessary requirement for applications towards commercial sensors.

The optimized interplay of these properties of CuO-NPs layers create an interesting possibility for the implementation towards the development of work function readout based CO_2 gas sensors (gas FETs) operated at room temperature.

Acknowledgements

Notes and references

1 (a) Y. Liu, J. Parisi, X. Sun and Y. Lei, *J. Mater. Chem. A*, 2014, **2**, 9919–9943; (b) D. J. Wales, J. Grand, V. P. Ting, R. D. Burke, K. J. Edler, C. R. Bowen, S. Mintova and A. D. Burrows, *Chem. Soc. Rev.*, 2015, **44**, 4290–4321; (c) G. Eranna, B. C. Joshi, D. P. Runthala and R. P. Gupta, *Crit. Rev. Solid State Mater. Sci.*, 2004, **29**, 111–188.

2 G. F. Fine, L. M. Cavanagh, A. Afonja and R. Binions, *Sensors*, 2010, **10**, 5469–5502.

3 (a) T. Ishihara, M. Higuchi, T. Takagi, M. Ito, H. Nishiguchi and Y. Takita, *J. Mater. Chem.*, 1998, **8**, 2037–2042; (b) H. Zhang, S. Wang, Y. Wang, J. Yang, X. Gao and L. Wang, *Phys. Chem. Chem. Phys.*, 2014, **16**, 10830.

4 M. Fleischer, *Meas. Sci. Technol.*, 2008, **19**, 42001.

5 (a) P. T. Moseley, J. O. W. Norris and D. E. Williams, *Techniques and Mechanisms in Gas Sensing*, Adam Hilger, Bristol, England, Philadelphia, 1991; (b) E. Della Gaspera, M. Guglielmi, S. Agnoli, G. Granozzi, M. L. Post, V. Bello, G. Mattei and A. Martucci, *Chem. Mater.*, 2010, **22**, 3407–3417; (c) L. G. Bloor, J. Manzi, R. Binions, I. P. Parkin, D. Pugh, A. Afonja, C. S. Blackman, S. Sathasivam and C. J. Carmalt, *Chem. Mater.*, 2012, **24**, 2864–2871; (d) S. Bai, K. Zhang, R. Luo, D. Li, A. Chen and C. C. Liu, *J. Mater. Chem.*, 2012, **22**, 12643; (e) X. Liu, Z. Chang, L. Luo, X. Lei, J. Liu and X. Sun, *J. Mater. Chem.*, 2012, **22**, 7232.

6 A. Marsal, G. Dezanneau, A. Cornet and J. R. Morante, *Sens. Actuators, B*, 2003, **95**, 266–270.

7 I. Djerdj, A. Haensch, D. Koziej, S. Pokhrel, N. Barsan, U. Weimar and M. Niederberger, *Chem. Mater.*, 2009, **21**, 5375–5381.

8 D. D. Trung, D. Le Toan, H. S. Hong, T. D. Lam, T. Trung and N. van Hieu, *Talanta*, 2012, **88**, 152–159.

9 K. Fan, H. Qin, L. Wang, L. Ju and J. Hu, *Sens. Actuators, B*, 2013, **177**, 265–269.

10 (a) W. Hong, Y. Chen, X. Feng, Y. Yan, X. Hu, B. Zhao, F. Zhang, D. Zhang, Z. Xu and Y. Lai, *Chem. Commun.*, 2013, **49**, 8229; (b) G. Korotcenkov, *Mater. Sci. Eng., B*, 2007, **139**, 1–23; (c) G. Sberveglieri, *Gas sensors. Principles, Operation and Developments*, Springer Science+Business Media Dordrecht, 1992; (d) M. Thompson and D. C. Stone, *Surface-launched Acoustic Wave Sensors. Chemical Sensing and Thin-film Characterization*, Wiley, New York, 1997, vol.144; (e) J. N. Zemel, *Rev. Sci. Instrum.*, 1990, **61**, 1579.

11 A.-M. Andringa, C. Piliego, I. Katsouras, P. W. M. Blom and D. M. d. Leeuw, *Chem. Mater.*, 2014, **26**, 773–785.

12 I. Lundström, S. Shivaraman, C. Svensson and L. Lundkvist, *Appl. Phys. Lett.*, 1975, **26**, 55.

13 A. Oprea, N. Bârsan and U. Weimar, *Sens. Actuators, B*, 2009, **142**, 470–493.

14 P. Davydovskaya, A. Ranft, B. V. Lotsch and R. Pohle, *Anal. Chem.*, 2014, **86**, 6948–6958.

15 P. Davydovskaya, R. Pohle, A. Tawil and M. Fleischer, *Sens. Actuators, B*, 2013, **187**, 142–146.

16 V. Pentyala, P. Davydovskaya, M. Ade, R. Pohle and G. Urban, *Sens. Actuators, B*, 2016, **222**, 904–909.

17 M. Holzinger, J. Maier and W. Sitte, *Papers from the International Workshop*, 1997, 94, pp. 217–225.

18 B. Ostrick, J. Mühlsteff, M. Fleischer, H. Meixner, T. Doll and C.-D. Kohl, *Sens. Actuators, B*, 1999, **57**, 115–119.

19 S. Stegmeier, M. Fleischer, A. Tawil, P. Hauptmann and H.-E. Endres, *Sens. Actuators, B*, 2011, **154**, 206–212.

20 L. M. Cavanagh and R. Binions, *Proc. IEEE Sens.*, 2011, 1006–1009.

21 T. Hibino and H. Iwahara, *Sens. Actuators, B*, 1993, **13**, 483–485.

22 D. Gibson and C. MacGregor, *Sensors*, 2013, **13**, 7079–7103.

23 N. B. Tanvir, C. Wilbertz, S. Steinhauer, A. Köck, G. Urban and O. Yurchenko, *Mater. Today Proc.*, 2015, **2**, 4190–4195.

24 N. B. Tanvir, O. Yurchenko and G. Urban, *Procedia Eng.*, 2015, **120**, 667–670.

This journal is © The Royal Society of Chemistry 2016

J. Mater. Chem. A, 2016, **4**, 5294–5302 | 5301

25 J. P. Joshua, S. Krishnan, D. V. Raj, R. Uthrakumar, S. Laxmi and S. J. Das, *Int. J. ChemTech Res.*, 2014, **6**, 2002–2004.

26 D. Amalric-Popescu and F. Bozon-Verduraz, *Catal. Today*, 2001, **70**, 139–154.

27 Z.-Z. Yang, Y.-N. Zhao and L.-N. He, *RSC Adv.*, 2011, **1**, 545.

28 R. Dhahri, M. Hjiri, L. El Mir, E. Fazio, F. Neri, F. Barreca, N. Donato, A. Bonavita, S. G. Leonardi and G. Neri, *J. Phys. D: Appl. Phys.*, 2015, **48**, 255503.

29 N. Barsan, M. Schweizer-Berberich and W. Göpel, *Fresenius. J. Anal. Chem.*, 1999, **365**, 287–304.

30 E. Garrone and C. Otero Areán, *Chem. Soc. Rev.*, 2005, **34**, 846.

31 C. Wang, L. Yin, L. Zhang, D. Xiang and R. Gao, *Sensors*, 2010, **10**, 2088.

32 A. Azam, *Int. J. Nanomed.*, 2012, **7**, 3527–3535.

33 (*a*) M. E. Böttcher, P. L. Gehlken, H. Skogby and C. Reutel, *Mineral. Mag.*, 1997, **61**, 249–256; (*b*) K. M. Dontsova, L. D. Norton, C. T. Johnston and J. M. Bigham, *Soil Sci. Soc. Am. J.*, 2004, **68**, 1218; (*c*) H. Gao, G. Wang, M. Yang, L. Tan and J. Yu, *Nanotechnology*, 2012, **23**, 15607.

34 I. Brown, K. Mackenzie and G. J. Gainsford, *Thermochim. Acta*, 1984, **75**, 23–32.

35 N. Barsan and U. Weimar, *J. Electroceram.*, 2001, **7**, 143–167.

36 M. Hübner, C. E. Simion, A. Tomescu-Stănoiu, S. Pokhrel, N. Bârsan and U. Weimar, *Sens. Actuators, B*, 2011, **153**, 347–353.

37 B. Ostrick, M. Fleischer, H. Meixner and C.-D. Kohl, *Sens. Actuators, B*, 2000, **68**, 197–202.

38 W. Preis and H. Gamsjäger, *Chem. Mon.*, 2001, **132**, 1327–1346.

39 *CRC Handbook of Chemistry and Physics*, ed. D. R. Lide, CRC, Boca Raton, FL, 2003rd edn, 2003.

40 W. Hummel, U. Berner, E. Curti, F. J. Pearson and T. Thoenen, *Radiochim. Acta*, 2002, **90**, 805–813.

41 W. N. R. W. Isahak, Z. A. C. Ramli, M. W. Ismail, K. Ismail, R. M. Yusop, M. W. M. Hisham and M. A. Yarmo, *J. CO$_2$ Util.*, 2013, **2**, 8–15.

42 H. Seidel, H. Ehrhardt, K. Viswanathan and W. Johannes, *Z. Anorg. Allg. Chem.*, 1974, **410**, 138–148.

43 B. W. Vink, *Mineral. Mag.*, 1986, **50**, 41–47.

44 V. Pentyala, P. Davydovskaya, M. Ade, R. Pohle and G. Urban, *Sens. Actuators, B*, 2016, **225**, 363–368.

45 V. Pentyala, P. Davydovskaya, R. Pohle, G. Urban and O. Yurchenko, *Procedia Eng.*, 2014, **87**, 1071–1074.

46 E. Laubender, N. B. Tanvir, O. Yurchenko and G. Urban, *Procedia Eng.*, 2015, **120**, 1058–1062.

5302 | *J. Mater. Chem. A*, 2016, **4**, 5294–5302

This journal is © The Royal Society of Chemistry 2016